

**Improved measurement of the decays $\eta' \rightarrow \pi^+ \pi^- \pi^+(0) \pi^-(0)$
and search for the rare decay $\eta' \rightarrow 4\pi^0$**

M. Ablikim,¹ M. N. Achasov,^{4,b} P. Adlarson,⁷⁵ X. C. Ai,⁸⁰ R. Aliberti,³⁵ A. Amoroso,^{74a,74c} M. R. An,³⁹ Q. An,^{71,58} Y. Bai,⁵⁷ O. Bakina,³⁶ I. Balossino,^{29a} Y. Ban,^{46,g} H.-R. Bao,⁶³ V. Batozskaya,^{1,44} K. Begzsuren,³² N. Berger,³⁵ M. Berlowski,⁴⁴ M. Bertani,^{28a} D. Bettoni,^{29a} F. Bianchi,^{74a,74c} E. Bianco,^{74a,74c} A. Bortone,^{74a,74c} I. Boyko,⁵⁶ R. A. Briere,⁵ A. Brueggemann,⁶⁸ H. Cai,⁷⁶ X. Cai,^{1,58} A. Calcaterra,^{28a} G. F. Cao,^{1,63} N. Cao,^{1,63} S. A. Cetin,^{62a} J. F. Chang,^{1,58} W. L. Chang,^{1,63} G. R. Che,⁴³ G. Chelkov,^{36,a} C. Chen,⁴³ Chao Chen,⁵⁵ G. Chen,¹ H. S. Chen,^{1,63} M. L. Chen,^{1,58,63} S. J. Chen,⁴² S. L. Chen,⁴⁵ S. M. Chen,⁶¹ T. Chen,^{1,63} X. R. Chen,^{31,63} X. T. Chen,^{1,63} Y. B. Chen,^{1,58} Y. Q. Chen,³⁴ Z. J. Chen,^{25,h} S. K. Choi,¹⁰ X. Chu,⁴³ G. Cibinetto,^{29a} S. C. Coen,³ F. Cossio,^{74c} J. J. Cui,⁵⁰ H. L. Dai,^{1,58} J. P. Dai,⁷⁸ A. Dbeysyi,¹⁸ R. E. de Boer,³ D. Dedovich,³⁶ Z. Y. Deng,¹ A. Denig,³⁵ I. Denysenko,³⁶ M. Destefanis,^{74a,74c} F. De Mori,^{74a,74c} B. Ding,^{66,1} X. X. Ding,^{46,g} Y. Ding,³⁴ Y. Ding,⁴⁰ J. Dong,^{1,58} L. Y. Dong,^{1,63} M. Y. Dong,^{1,58,63} X. Dong,⁷⁶ M. C. Du,¹ S. X. Du,⁸⁰ Z. H. Duan,⁴² P. Egorov,^{36,a} Y. H. Fan,⁴⁵ J. Fang,^{1,58} S. S. Fang,^{1,63} W. X. Fang,¹ Y. Fang,¹ Y. Q. Fang,^{1,58} R. Farinelli,^{29a} L. Fava,^{74b,74c} F. Feldbauer,³ G. Felici,^{28a} C. Q. Feng,^{71,58} J. H. Feng,⁵⁹ Y. T. Feng,⁷¹ K. Fischer,⁶⁹ M. Fritsch,³ C. D. Fu,¹ J. L. Fu,⁶³ Y. W. Fu,¹ H. Gao,⁶³ Y. N. Gao,^{46,g} Yang Gao,^{71,58} S. Garbolino,^{74c} I. Garzia,^{29a,29b} P. T. Ge,⁷⁶ Z. W. Ge,⁴² C. Geng,⁵⁹ E. M. Gersabeck,⁶⁷ A. Gilman,⁶⁹ K. Goetzen,¹³ L. Gong,⁴⁰ W. X. Gong,^{1,58} W. Gradl,³⁵ S. Gramigna,^{29a,29b} M. Greco,^{74a,74c} M. H. Gu,^{1,58} Y. T. Gu,¹⁵ C. Y. Guan,^{1,63} Z. L. Guan,²² A. Q. Guo,^{31,63} L. B. Guo,⁴¹ M. J. Guo,⁵⁰ R. P. Guo,⁴⁹ Y. P. Guo,^{12,f} A. Guskov,^{36,a} J. Gutierrez,²⁷ K. L. Han,⁶³ T. T. Han,¹ W. Y. Han,³⁹ X. Q. Hao,¹⁹ F. A. Harris,⁶⁵ K. K. He,⁵⁵ K. L. He,^{1,63} F. H. H. Heinsius,³ C. H. Heinz,³⁵ Y. K. Heng,^{1,58,63} C. Herold,⁶⁰ T. Holtmann,³ P. C. Hong,^{12,f} G. Y. Hou,^{1,63} X. T. Hou,^{1,63} Y. R. Hou,⁶³ Z. L. Hou,¹ B. Y. Hu,⁵⁹ H. M. Hu,^{1,63} J. F. Hu,^{56,i} T. Hu,^{1,58,63} Y. Hu,¹ G. S. Huang,^{71,58} K. X. Huang,⁵⁹ L. Q. Huang,^{31,63} X. T. Huang,⁵⁰ Y. P. Huang,¹ T. Hussain,⁷³ N. Hüsken,^{27,35} N. in der Wiesche,⁶⁸ M. Irshad,^{71,58} J. Jackson,²⁷ S. Jaeger,³ S. Janchiv,³² J. H. Jeong,¹⁰ Q. Ji,¹ Q. P. Ji,¹⁹ X. B. Ji,^{1,63} X. L. Ji,^{1,58} Y. Y. Ji,⁵⁰ X. Q. Jia,⁵⁰ Z. K. Jia,^{71,58} H. B. Jiang,⁷⁶ P. C. Jiang,^{46,g} S. S. Jiang,³⁹ T. J. Jiang,¹⁶ X. S. Jiang,^{1,58,63} Y. Jiang,⁶³ J. B. Jiao,⁵⁰ Z. Jiao,²³ S. Jin,⁴² Y. Jin,⁶⁶ M. Q. Jing,^{1,63} X. M. Jing,⁶³ T. Johansson,⁷⁵ X. K.,¹ S. Kabana,³³ N. Kalantar-Nayestanaki,⁶⁴ X. L. Kang,⁹ X. S. Kang,⁴⁰ M. Kavatsyuk,⁶⁴ B. C. Ke,⁸⁰ V. Khachatryan,²⁷ A. Khoukaz,⁶⁸ R. Kiuchi,¹ O. B. Kolcu,^{62a} B. Kopf,³ M. Kuessner,³ A. Kupsc,^{44,75} W. Kühn,³⁷ J. J. Lane,⁶⁷ P. Larin,¹⁸ L. Lavezzi,^{74a,74c} T. T. Lei,^{71,58} Z. H. Lei,^{71,58} H. Leithoff,³⁵ M. Lellmann,³⁵ T. Lenz,³⁵ C. Li,⁴⁷ C. Li,⁴³ C. H. Li,³⁹ Cheng Li,^{71,58} D. M. Li,⁸⁰ F. Li,^{1,58} G. Li,¹ H. Li,^{71,58} H. B. Li,^{1,63} H. J. Li,¹⁹ H. N. Li,^{56,i} Hui Li,⁴³ J. R. Li,⁶¹ J. S. Li,⁵⁹ J. W. Li,⁵⁰ Ke Li,¹ L. J. Li,^{1,63} L. K. Li,¹ Lei Li,⁴⁸ M. H. Li,⁴³ P. R. Li,^{38,k} Q. X. Li,⁵⁰ S. X. Li,¹² T. Li,⁵⁰ W. D. Li,^{1,63} W. G. Li,¹ X. H. Li,^{71,58} X. L. Li,⁵⁰ Xiaoyu Li,^{1,63} Y. G. Li,^{46,g} Z. J. Li,⁵⁹ Z. X. Li,¹⁵ C. Liang,⁴² H. Liang,^{1,63} H. Liang,^{71,58} Y. F. Liang,⁵⁴ Y. T. Liang,^{31,63} G. R. Liao,¹⁴ L. Z. Liao,⁵⁰ Y. P. Liao,^{1,63} J. Libby,²⁶ A. Limphirat,⁶⁰ D. X. Lin,^{31,63} T. Lin,¹ B. J. Liu,¹ B. X. Liu,⁷⁶ C. Liu,³⁴ C. X. Liu,¹ F. H. Liu,⁵³ Fang Liu,¹ Feng Liu,⁶ G. M. Liu,^{56,i} H. Liu,^{38,j,k} H. B. Liu,¹⁵ H. M. Liu,^{1,63} Huanhuan Liu,¹ Huihui Liu,²¹ J. B. Liu,^{71,58} J. Y. Liu,^{1,63} K. Liu,^{38,j,k} K. Y. Liu,⁴⁰ Ke Liu,²² L. Liu,^{71,58} L. C. Liu,⁴³ Lu Liu,⁴³ M. H. Liu,^{12,f} P. L. Liu,¹ Q. Liu,⁶³ S. B. Liu,^{71,58} T. Liu,^{12,f} W. K. Liu,⁴³ W. M. Liu,^{71,58} X. Liu,^{38,j,k} Y. Liu,⁸⁰ Y. Liu,^{38,j,k} Y. B. Liu,⁴³ Z. A. Liu,^{1,58,63} Z. Q. Liu,⁵⁰ X. C. Lou,^{1,58,63} F. X. Lu,⁵⁹ H. J. Lu,²³ J. G. Lu,^{1,58} X. L. Lu,¹ Y. Lu,⁷ Y. P. Lu,^{1,58} Z. H. Lu,^{1,63} C. L. Luo,⁴¹ M. X. Luo,⁷⁹ T. Luo,^{12,f} X. L. Luo,^{1,58} X. R. Lyu,⁶³ Y. F. Lyu,⁴³ F. C. Ma,⁴⁰ H. Ma,⁷⁸ H. L. Ma,¹ J. L. Ma,^{1,63} L. L. Ma,⁵⁰ M. M. Ma,^{1,63} Q. M. Ma,¹ R. Q. Ma,^{1,63} X. Y. Ma,^{1,58} Y. Ma,^{46,g} Y. M. Ma,³¹ F. E. Maas,¹⁸ M. Maggiora,^{74a,74c} S. Malde,⁶⁹ Q. A. Malik,⁷³ A. Mangoni,^{28b} Y. J. Mao,^{46,g} Z. P. Mao,¹ S. Marcello,^{74a,74c} Z. X. Meng,⁶⁶ J. G. Messchendorp,^{13,64} G. Mezzadri,^{29a} H. Miao,^{1,63} T. J. Min,⁴² R. E. Mitchell,²⁷ X. H. Mo,^{1,58,63} B. Moses,²⁷ N. Yu. Muchnoi,^{4,b} J. Muskalla,³⁵ Y. Nefedov,³⁶ F. Nerling,^{18,d} I. B. Nikolaev,^{4,b} Z. Ning,^{1,58} S. Nisar,^{11,1} Q. L. Niu,^{38,j,k} W. D. Niu,⁵⁵ Y. Niu,⁵⁰ S. L. Olsen,⁶³ Q. Ouyang,^{1,58,63} S. Pacetti,^{28b,28c} X. Pan,⁵⁵ Y. Pan,⁵⁷ A. Pathak,³⁴ P. Patteri,^{28a} Y. P. Pei,^{71,58} M. Pelizaeus,³ H. P. Peng,^{71,58} Y. Y. Peng,^{38,j,k} K. Peters,^{13,d} J. L. Ping,⁴¹ R. G. Ping,^{1,63} S. Plura,³⁵ V. Prasad,³³ F. Z. Qi,¹ H. Qi,^{71,58} H. R. Qi,⁶¹ M. Qi,⁴² T. Y. Qi,^{12,f} S. Qian,^{1,58} W. B. Qian,⁶³ C. F. Qiao,⁶³ J. J. Qin,⁷² L. Q. Qin,¹⁴ X. S. Qin,⁵⁰ Z. H. Qin,^{1,58} J. F. Qiu,¹ S. Q. Qu,⁶¹ C. F. Redmer,³⁵ K. J. Ren,³⁹ A. Rivetti,^{74c} M. Rolo,^{74c} G. Rong,^{1,63} Ch. Rosner,¹⁸ S. N. Ruan,⁴³ N. Salone,⁴⁴ A. Sarantsev,^{36,c} Y. Schelhaas,³⁵ K. Schoenning,⁷⁵ M. Scodreggio,^{29a,29b} K. Y. Shan,^{12,f} W. Shan,²⁴ X. Y. Shan,^{71,58} J. F. Shanguan,⁵⁵ L. G. Shao,^{1,63} M. Shao,^{71,58} C. P. Shen,^{12,f} H. F. Shen,^{1,63} W. H. Shen,⁶³ X. Y. Shen,^{1,63} B. A. Shi,⁶³ H. C. Shi,^{71,58} J. L. Shi,¹² J. Y. Shi,¹ Q. Q. Shi,⁵⁵ R. S. Shi,^{1,63} X. Shi,^{1,58} J. J. Song,¹⁹ T. Z. Song,⁵⁹ W. M. Song,^{34,1} Y. J. Song,¹² S. Sosio,^{74a,74c} S. Spataro,^{74a,74c} F. Stieler,³⁵ Y. J. Su,⁶³ G. B. Sun,⁷⁶ G. X. Sun,¹ H. Sun,⁶³ H. K. Sun,¹ J. F. Sun,¹⁹ K. Sun,⁶¹ L. Sun,⁷⁶ S. S. Sun,^{1,63} T. Sun,^{51,e} W. Y. Sun,³⁴ Y. Sun,⁹ Y. J. Sun,^{71,58} Y. Z. Sun,¹ Z. T. Sun,⁵⁰ Y. X. Tan,^{71,58} C. J. Tang,⁵⁴ G. Y. Tang,¹ J. Tang,⁵⁹ Y. A. Tang,⁷⁶ L. Y. Tao,⁷² Q. T. Tao,^{25,h} M. Tat,⁶⁹ J. X. Teng,^{71,58} V. Thoren,⁷⁵ W. H. Tian,⁵² W. H. Tian,⁵⁹ Y. Tian,^{31,63} Z. F. Tian,⁷⁶

I. Uman,^{62b} Y. Wan,⁵⁵ S. J. Wang,⁵⁰ B. Wang,¹ B. L. Wang,⁶³ Bo Wang,^{71,58} C. W. Wang,⁴² D. Y. Wang,^{46,g} F. Wang,⁷² H. J. Wang,^{38,j,k} J. P. Wang,⁵⁰ K. Wang,^{1,58} L. L. Wang,¹ M. Wang,⁵⁰ Meng Wang,^{1,63} N. Y. Wang,⁶³ S. Wang,^{38,j,k} S. Wang,^{12,f} T. Wang,^{12,f} T. J. Wang,⁴³ W. Wang,⁵⁹ W. Wang,⁷² W. P. Wang,^{71,58} X. Wang,^{46,g} X. F. Wang,^{38,j,k} X. J. Wang,³⁹ X. L. Wang,^{12,f} Y. Wang,⁶¹ Y. D. Wang,⁴⁵ Y. F. Wang,^{1,58,63} Y. L. Wang,¹⁹ Y. N. Wang,⁴⁵ Y. Q. Wang,¹ Yaqian Wang,^{17,1} Yi Wang,⁶¹ Z. Wang,^{1,58} Z. L. Wang,⁷² Z. Y. Wang,^{1,63} Ziyi Wang,⁶³ D. Wei,⁷⁰ D. H. Wei,¹⁴ F. Weidner,⁶⁸ S. P. Wen,¹ C. W. Wenzel,³ U. Wiedner,³ G. Wilkinson,⁶⁹ M. Wolke,⁷⁵ L. Wollenberg,³ C. Wu,³⁹ J. F. Wu,^{1,8} L. H. Wu,¹ L. J. Wu,^{1,63} X. Wu,^{12,f} X. H. Wu,³⁴ Y. Wu,⁷¹ Y. H. Wu,⁵⁵ Y. J. Wu,³¹ Z. Wu,^{1,58} L. Xia,^{71,58} X. M. Xian,³⁹ T. Xiang,^{46,g} D. Xiao,^{38,j,k} G. Y. Xiao,⁴² S. Y. Xiao,¹ Y. L. Xiao,^{12,f} Z. J. Xiao,⁴¹ C. Xie,⁴² X. H. Xie,^{46,g} Y. Xie,⁵⁰ Y. G. Xie,^{1,58} Y. H. Xie,⁶ Z. P. Xie,^{71,58} T. Y. Xing,^{1,63} C. F. Xu,^{1,63} C. J. Xu,⁵⁹ G. F. Xu,¹ H. Y. Xu,⁶⁶ Q. J. Xu,¹⁶ Q. N. Xu,³⁰ W. Xu,¹ W. L. Xu,⁶⁶ X. P. Xu,⁵⁵ Y. C. Xu,⁷⁷ Z. P. Xu,⁴² Z. S. Xu,⁶³ F. Yan,^{12,f} L. Yan,^{12,f} W. B. Yan,^{71,58} W. C. Yan,⁸⁰ X. Q. Yan,¹ H. J. Yang,^{51,e} H. L. Yang,³⁴ H. X. Yang,¹ Tao Yang,¹ Y. Yang,^{12,f} Y. F. Yang,⁴³ Y. X. Yang,^{1,63} Yifan Yang,^{1,63} Z. W. Yang,^{38,j,k} Z. P. Yao,⁵⁰ M. Ye,^{1,58} M. H. Ye,⁸ J. H. Yin,¹ Z. Y. You,⁵⁹ B. X. Yu,^{1,58,63} C. X. Yu,⁴⁵ G. Yu,^{1,63} J. S. Yu,^{25,h} T. Yu,⁷² X. D. Yu,^{46,g} C. Z. Yuan,^{1,63} L. Yuan,² S. C. Yuan,¹ Y. Yuan,^{1,63} Z. Y. Yuan,⁵⁹ C. X. Yue,³⁹ A. A. Zafar,⁷³ F. R. Zeng,⁵⁰ S. H. Zeng,⁷² X. Zeng,^{12,f} Y. Zeng,^{25,h} Y. J. Zeng,^{1,63} X. Y. Zhai,³⁴ Y. C. Zhai,⁵⁰ Y. H. Zhan,⁵⁹ A. Q. Zhang,^{1,63} B. L. Zhang,^{1,63} B. X. Zhang,¹ D. H. Zhang,⁴³ G. Y. Zhang,¹⁹ H. Zhang,⁷¹ H. C. Zhang,^{1,58,63} H. H. Zhang,⁵⁹ H. H. Zhang,³⁴ H. Q. Zhang,^{1,58,63} H. Y. Zhang,^{1,58} J. Zhang,⁵⁹ J. Zhang,⁸⁰ J. J. Zhang,⁵² J. L. Zhang,²⁰ J. Q. Zhang,⁴¹ J. W. Zhang,^{1,58,63} J. X. Zhang,^{38,j,k} J. Y. Zhang,¹ J. Z. Zhang,^{1,63} Jianyu Zhang,⁶³ L. M. Zhang,⁶¹ L. Q. Zhang,⁵⁹ Lei Zhang,⁴² P. Zhang,^{1,63} Q. Y. Zhang,^{39,80} Shuihan Zhang,^{1,63} Shulei Zhang,^{25,h} X. D. Zhang,⁴⁵ X. M. Zhang,¹ X. Y. Zhang,⁵⁰ Y. Zhang,⁶⁹ Y. Zhang,⁷² Y. T. Zhang,⁸⁰ Y. H. Zhang,^{1,58} Yan Zhang,^{71,58} Yao Zhang,¹ Z. D. Zhang,¹ Z. H. Zhang,¹ Z. L. Zhang,³⁴ Z. Y. Zhang,⁷⁶ Z. Y. Zhang,⁴³ G. Zhao,¹ J. Y. Zhao,^{1,63} J. Z. Zhao,^{1,58} Lei Zhao,^{71,58} Ling Zhao,¹ M. G. Zhao,⁴³ R. P. Zhao,⁶³ S. J. Zhao,⁸⁰ Y. B. Zhao,^{1,58} Y. X. Zhao,^{31,63} Z. G. Zhao,^{71,58} Z. H. Zhao,¹⁹ A. Zhemchugov,^{36,a} B. Zheng,⁷² J. P. Zheng,^{1,58} W. J. Zheng,^{1,63} Y. H. Zheng,⁶³ B. Zhong,⁴¹ X. Zhong,⁵⁹ H. Zhou,⁵⁰ L. P. Zhou,^{1,63} X. Zhou,⁷⁶ X. K. Zhou,⁶ X. R. Zhou,^{71,58} X. Y. Zhou,³⁹ Y. Z. Zhou,^{12,f} J. Zhu,⁴³ K. Zhu,¹ K. J. Zhu,^{1,58,63} L. Zhu,³⁴ L. X. Zhu,⁶³ S. H. Zhu,⁷⁰ S. Q. Zhu,⁴² T. J. Zhu,^{12,f} W. J. Zhu,^{12,f} Y. C. Zhu,^{71,58} Z. A. Zhu,^{1,63} J. H. Zou,¹ and J. Zu^{71,58}

(BESIII Collaboration)

¹*Institute of High Energy Physics, Beijing 100049, People's Republic of China*²*Beihang University, Beijing 100191, People's Republic of China*³*Bochum Ruhr-University, D-44780 Bochum, Germany*⁴*Budker Institute of Nuclear Physics SB RAS (BINP), Novosibirsk 630090, Russia*⁵*Carnegie Mellon University, Pittsburgh, Pennsylvania 15213, USA*⁶*Central China Normal University, Wuhan 430079, People's Republic of China*⁷*Central South University, Changsha 410083, People's Republic of China*⁸*China Center of Advanced Science and Technology, Beijing 100190, People's Republic of China*⁹*China University of Geosciences, Wuhan 430074, People's Republic of China*¹⁰*Chung-Ang University, Seoul 06974, Republic of Korea*¹¹*COMSATS University Islamabad, Lahore Campus, Defence Road, Off Raiwind Road, 54000 Lahore, Pakistan*¹²*Fudan University, Shanghai 200433, People's Republic of China*¹³*GSI Helmholtzcentre for Heavy Ion Research GmbH, D-64291 Darmstadt, Germany*¹⁴*Guangxi Normal University, Guilin 541004, People's Republic of China*¹⁵*Guangxi University, Nanning 530004, People's Republic of China*¹⁶*Hangzhou Normal University, Hangzhou 310036, People's Republic of China*¹⁷*Hebei University, Baoding 071002, People's Republic of China*¹⁸*Helmholtz Institute Mainz, Staudinger Weg 18, D-55099 Mainz, Germany*¹⁹*Henan Normal University, Xinxiang 453007, People's Republic of China*²⁰*Henan University, Kaifeng 475004, People's Republic of China*²¹*Henan University of Science and Technology, Luoyang 471003, People's Republic of China*²²*Henan University of Technology, Zhengzhou 450001, People's Republic of China*²³*Huangshan College, Huangshan 245000, People's Republic of China*²⁴*Hunan Normal University, Changsha 410081, People's Republic of China*²⁵*Hunan University, Changsha 410082, People's Republic of China*²⁶*Indian Institute of Technology Madras, Chennai 600036, India*²⁷*Indiana University, Bloomington, Indiana 47405, USA*

- ^{28a}INFN Laboratori Nazionali di Frascati, I-00044, Frascati, Italy
^{28b}INFN Sezione di Perugia, I-06100, Perugia, Italy
^{28c}University of Perugia, I-06100 Perugia, Italy
^{29a}INFN Sezione di Ferrara, I-44122 Ferrara, Italy
^{29b}University of Ferrara, I-44122 Ferrara, Italy
³⁰Inner Mongolia University, Hohhot 010021, People's Republic of China
³¹Institute of Modern Physics, Lanzhou 730000, People's Republic of China
³²Institute of Physics and Technology, Peace Avenue 54B, Ulaanbaatar 13330, Mongolia
³³Instituto de Alta Investigación, Universidad de Tarapacá, Casilla 7D, Arica 1000000, Chile
³⁴Jilin University, Changchun 130012, People's Republic of China
³⁵Johannes Gutenberg University of Mainz, Johann-Joachim-Becher-Weg 45, D-55099 Mainz, Germany
³⁶Joint Institute for Nuclear Research, 141980 Dubna, Moscow region, Russia
³⁷Justus-Liebig-Universitaet Giessen, II. Physikalisches Institut, Heinrich-Buff-Ring 16, D-35392 Giessen, Germany
³⁸Lanzhou University, Lanzhou 730000, People's Republic of China
³⁹Liaoning Normal University, Dalian 116029, People's Republic of China
⁴⁰Liaoning University, Shenyang 110036, People's Republic of China
⁴¹Nanjing Normal University, Nanjing 210023, People's Republic of China
⁴²Nanjing University, Nanjing 210093, People's Republic of China
⁴³Nankai University, Tianjin 300071, People's Republic of China
⁴⁴National Centre for Nuclear Research, Warsaw 02-093, Poland
⁴⁵North China Electric Power University, Beijing 102206, People's Republic of China
⁴⁶Peking University, Beijing 100871, People's Republic of China
⁴⁷Qufu Normal University, Qufu 273165, People's Republic of China
⁴⁸Renmin University of China, Beijing 100872, People's Republic of China
⁴⁹Shandong Normal University, Jinan 250014, People's Republic of China
⁵⁰Shandong University, Jinan 250100, People's Republic of China
⁵¹Shanghai Jiao Tong University, Shanghai 200240, People's Republic of China
⁵²Shanxi Normal University, Linfen 041004, People's Republic of China
⁵³Shanxi University, Taiyuan 030006, People's Republic of China
⁵⁴Sichuan University, Chengdu 610064, People's Republic of China
⁵⁵Soochow University, Suzhou 215006, People's Republic of China
⁵⁶South China Normal University, Guangzhou 510006, People's Republic of China
⁵⁷Southeast University, Nanjing 211100, People's Republic of China
⁵⁸State Key Laboratory of Particle Detection and Electronics, Beijing 100049, Hefei 230026, People's Republic of China
⁵⁹Sun Yat-Sen University, Guangzhou 510275, People's Republic of China
⁶⁰Suranaree University of Technology, University Avenue 111, Nakhon Ratchasima 30000, Thailand
⁶¹Tsinghua University, Beijing 100084, People's Republic of China
^{62a}Turkish Accelerator Center Particle Factory Group, Istinye University, 34010 Istanbul, Turkey
^{62b}Near East University, Nicosia, North Cyprus, 99138 Mersin 10, Turkey
⁶³University of Chinese Academy of Sciences, Beijing 100049, People's Republic of China
⁶⁴University of Groningen, NL-9747 AA Groningen, The Netherlands
⁶⁵University of Hawaii, Honolulu, Hawaii 96822, USA
⁶⁶University of Jinan, Jinan 250022, People's Republic of China
⁶⁷University of Manchester, Oxford Road, Manchester M13 9PL, United Kingdom
⁶⁸University of Muenster, Wilhelm-Klemm-Strasse 9, 48149 Muenster, Germany
⁶⁹University of Oxford, Keble Road, Oxford OX13RH, United Kingdom
⁷⁰University of Science and Technology Liaoning, Anshan 114051, People's Republic of China
⁷¹University of Science and Technology of China, Hefei 230026, People's Republic of China
⁷²University of South China, Hengyang 421001, People's Republic of China
⁷³University of the Punjab, Lahore-54590, Pakistan
^{74a}University of Turin and INFN, University of Turin, I-10125 Turin, Italy
^{74b}University of Eastern Piedmont, I-15121 Alessandria, Italy
^{74c}INFN, I-10125 Turin, Italy
⁷⁵Uppsala University, Box 516, SE-75120 Uppsala, Sweden
⁷⁶Wuhan University, Wuhan 430072, People's Republic of China
⁷⁷Yantai University, Yantai 264005, People's Republic of China

⁷⁸Yunnan University, Kunming 650500, People's Republic of China
⁷⁹Zhejiang University, Hangzhou 310027, People's Republic of China
⁸⁰Zhengzhou University, Zhengzhou 450001, People's Republic of China



(Received 23 November 2023; accepted 23 January 2024; published 16 February 2024)

Using a sample of 10 billion J/ψ events collected with the BESIII detector, the decays $\eta' \rightarrow \pi^+\pi^-\pi^+\pi^-$, $\eta' \rightarrow \pi^+\pi^-\pi^0\pi^0$ and $\eta' \rightarrow 4\pi^0$ are studied via the process $J/\psi \rightarrow \gamma\eta'$. The branching fractions of $\eta' \rightarrow \pi^+\pi^-\pi^+\pi^-$ and $\eta' \rightarrow \pi^+\pi^-\pi^0\pi^0$ are measured to be $(8.56 \pm 0.25(\text{stat}) \pm 0.23(\text{syst})) \times 10^{-5}$ and $(2.12 \pm 0.12(\text{stat}) \pm 0.10(\text{syst})) \times 10^{-4}$, respectively, which are consistent with previous measurements but with improved precision. No significant $\eta' \rightarrow 4\pi^0$ signal is observed, and the upper limit on the branching fraction of this decay is determined to be less than 1.24×10^{-5} at the 90% confidence level. In addition, an amplitude analysis of $\eta' \rightarrow \pi^+\pi^-\pi^+\pi^-$ is performed to extract the doubly virtual isovector form factor α for the first time. The measured value of $\alpha = 1.22 \pm 0.33(\text{stat}) \pm 0.04(\text{syst})$, is in agreement with the prediction of the vector meson dominance model.

DOI: 10.1103/PhysRevD.109.032006

I. INTRODUCTION

The η' meson, interpreted as a flavor singlet state arising from the axial U(1) anomaly, has attracted both theoretical and experimental attention due to its special role in helping to understand low-energy quantum chromodynamics (QCD).

^aAlso at the Moscow Institute of Physics and Technology, Moscow 141700, Russia.

^bAlso at the Novosibirsk State University, Novosibirsk 630090, Russia.

^cAlso at the NRC ‘‘Kurchatov Institute,’’ PNPI, 188300 Gatchina, Russia.

^dAlso at Goethe University Frankfurt, 60323 Frankfurt am Main, Germany.

^eAlso at Key Laboratory for Particle Physics, Astrophysics and Cosmology, Ministry of Education; Shanghai Key Laboratory for Particle Physics and Cosmology; and Institute of Nuclear and Particle Physics, Shanghai 200240, People's Republic of China.

^fAlso at Key Laboratory of Nuclear Physics and Ion-beam Application (MOE) and Institute of Modern Physics, Fudan University, Shanghai 200443, People's Republic of China.

^gAlso at State Key Laboratory of Nuclear Physics and Technology, Peking University, Beijing 100871, People's Republic of China.

^hAlso at School of Physics and Electronics, Hunan University, Changsha 410082, China.

ⁱAlso at Guangdong Provincial Key Laboratory of Nuclear Science, Institute of Quantum Matter, South China Normal University, Guangzhou 510006, China.

^jAlso at MOE Frontiers Science Center for Rare Isotopes, Lanzhou University, Lanzhou 730000, People's Republic of China.

^kAlso at Lanzhou Center for Theoretical Physics, Lanzhou University, Lanzhou 730000, People's Republic of China.

^lAlso at the Department of Mathematical Sciences, IBA, Karachi 75270, Pakistan.

Published by the American Physical Society under the terms of the Creative Commons Attribution 4.0 International license. Further distribution of this work must maintain attribution to the author(s) and the published article's title, journal citation, and DOI. Funded by SCOAP³.

Its dominant radiative and hadronic decays have been observed and well-measured, however the study of its rare decays is still an open field, and is of value for investigating the symmetry-breaking mechanisms and testing chiral perturbation theory (ChPT). In addition, η' decays also play an important role in the evaluation of the hadronic light-by-light contribution to the muon anomalous magnetic moment (see Refs. [1,2] for details).

The hadronic decays $\eta' \rightarrow \pi^+\pi^-\pi^+(0)\pi^-(0)$, where the pion pairs are formed by internal conversion of two intermediate virtual photons, are of special interest. Within the framework of the vector meson dominance (VMD) model, one can expect that each virtual photon converts mainly into a virtual ρ meson, which decays with large probability into two pions, despite the smaller available phase space. Therefore, the $\eta' \rightarrow \pi^+\pi^-\pi^+(0)\pi^-(0)$ channel can provide valuable information about the meson- $\gamma^*\gamma^*$ coupling, which is of importance for the calculation of the hadronic contribution to the anomalous magnetic moment of the muon. However, the information on such decays is scarce. In 2014, the BESIII Collaboration reported the first observation of $\eta' \rightarrow \pi^+\pi^-\pi^+(0)\pi^-(0)$ decays [3]. The measured branching fractions are in agreement with theoretical predictions [4], but an amplitude analysis of these decays was not performed due to the limited sample sizes.

Interest in the very rare decay $\eta' \rightarrow 4\pi^0$ stems from the S -wave CP -violation. As a result, this decay is highly suppressed and the S -wave CP -violating effect that contributes to this decay is at a level of 10^{-23} [5,6], which is beyond experimental accessibility. However, within the ChPT and VMD model, the branching fraction may reach a level of 10^{-8} through the presence of a D -wave contribution [4]. Several attempts have been made to search for this decay [7–9]. The most stringent upper limit of the branching fraction $\mathcal{B}(\eta' \rightarrow 4\pi^0) < 4.94 \times 10^{-5}$ at the 90% confidence level was set by the BESIII Collaboration, from an analysis based on a sample of 1.31×10^9 J/ψ events [9].

BESIII has now collected a dataset of $(10087 \pm 44) \times 10^6 J/\psi$ events [10], which allows for improved analyses of η' decaying into four pions and also the extraction of the timelike double virtual transition form factor (TFF) information of the η' meson. In this paper, we present studies of $\eta' \rightarrow \pi^+\pi^-\pi^+(0)\pi^-(0)$ and $\eta' \rightarrow 4\pi^0$ via the process $J/\psi \rightarrow \gamma\eta'$. In addition, an amplitude analysis of $\eta' \rightarrow \pi^+\pi^-\pi^+\pi^-$ is performed to extract the doubly virtual timelike form factor of η' within the framework of the combination of the ChPT and VMD model [4].

II. DETECTOR AND MONTE CARLO SAMPLES

The BESIII detector [11] records symmetric e^+e^- collisions provided by the BEPCII storage ring [12] in the center-of-mass energy range from 2.0 to 4.95 GeV, with a peak luminosity of $1.1 \times 10^{33} \text{ cm}^{-2} \text{ s}^{-1}$ achieved at $\sqrt{s} = 3.77 \text{ GeV}$. The BESIII detector has collected large data samples in this energy region [13]. The cylindrical core of the BESIII detector covers 93% of the full solid angle and comprises a helium-based multilayer drift chamber (MDC), a plastic scintillator time-of-flight system (TOF), and a CsI (TI) electromagnetic calorimeter (EMC), which are all enclosed in a superconducting solenoidal magnet providing a 1.0 T magnetic field. The solenoid is supported by an octagonal flux-return yoke with resistive plate counter muon identification modules interleaved with steel. The charged-particle momentum resolution at 1 GeV/c is 0.5%, and the dE/dx resolution is 6% for electrons from Bhabha scattering. The EMC measures photon energies with a resolution of 2.5% (5%) at 1 GeV in the barrel (end-cap) region. The time resolution in the TOF barrel region is 68 ps, while that in the end-cap region was 110 ps. The end cap TOF system was upgraded in 2015 using multigap resistive plate chamber technology, providing a time resolution of 60 ps.

Simulated data samples produced with a Geant4-based [14] Monte Carlo (MC) package, which includes the geometric description of the BESIII detector and the detector response, are used to determine the detection efficiencies and estimate backgrounds. The simulation models the beam-energy spread and initial-state radiation in the e^+e^- annihilations with the generator KKMC [15]. The inclusive MC sample of 10 billion J/ψ events consists of the production of J/ψ resonance, and the continuum processes incorporation in KKMC [15]. All particle decays are modeled with EvtGen [16] using branching fractions either taken from the Particle Data Group (PDG) [17], when available, or otherwise estimated with LUNDCHARM [18]. Final-state radiation from charged final-state particles is incorporated using the PHOTOS package [19]. Specific generators are employed for the three signal channels: $\eta' \rightarrow \pi^+\pi^-\pi^+(0)\pi^-(0)$ and $\eta' \rightarrow 4\pi^0$, which are based on the ChPT and VMD model [4].

III. EVENT SELECTION AND BACKGROUND ANALYSIS

Each charged track, reconstructed in the MDC, is required to originate from a region within 10 cm of the interaction point (IP) along the beam direction and 1 cm in the plane perpendicular to the beam. The polar angle θ of the tracks must be within the fiducial volume of the MDC $|\cos\theta| < 0.93$. Particle identification is not used for the charged tracks in this analysis. Neutral clusters are identified using showers in the EMC. The deposited energy of each shower must be more than 25 MeV in the barrel region ($|\cos\theta| < 0.8$) and more than 50 MeV in the end cap region ($0.86 < |\cos\theta| < 0.92$). The difference between the EMC time and the event start time [20] is required to be within (0, 700) ns for the decay modes $\eta' \rightarrow \pi^+\pi^-\pi^+(0)\pi^-(0)$, while the timing of the shower with respect to the most energetic photon must lie within (-500, 500) ns for the decay $\eta' \rightarrow 4\pi^0$ to suppress electronic noise and showers unrelated to the event.

For $J/\psi \rightarrow \gamma\eta'$ with $\eta' \rightarrow \pi^+\pi^-\pi^+\pi^-$ (Mode I), candidate events are required to have four charged tracks with net zero charge and at least one photon. The candidate events are required to successfully pass a vertex fit to the interaction point (IP). Then a four-constraint (4C) kinematic fit to the initial e^+e^- four momentum is performed under the $\gamma\pi^+\pi^-\pi^+\pi^-$ hypothesis. In events with more than one photon, all combinations are considered under this hypothesis and the combination with the smallest χ_{4C}^2 is retained for further analysis. To reject possible background events with one more photon, we further require that the probability of the 4C fit for the $\gamma\pi^+\pi^-\pi^+\pi^-$ assignment is greater than that for the $\gamma\gamma\pi^+\pi^-\pi^+\pi^-$ hypothesis. With the requirement of $\chi_{4C}^2 < 35$, the $\pi^+\pi^-\pi^+\pi^-$ mass spectrum is displayed in Fig. 1(a), where a clear η' peak is observed. To ensure that the η' peak originates from the signal process rather than background, the same analysis selection is performed with the inclusive MC sample of 10 billion J/ψ events. Detailed event-type analysis [21] over the surviving MC candidates indicates that the broad enhancement below the η' peak is from the background channel $\eta' \rightarrow \pi^+\pi^-\eta$ with $\eta \rightarrow \gamma\pi^+\pi^-$ and the region around 0.98 GeV/ c^2 receives contamination from $\eta' \rightarrow \pi^+\pi^-\mu^+\mu^-$ decays. The backgrounds in the mass region above 1 GeV/ c^2 are mainly from $\eta' \rightarrow \pi^+\pi^-e^+e^-$ and $\eta' \rightarrow \gamma\pi^+\pi^-$ events. The remaining nonresonant background events are from $J/\psi \rightarrow \gamma\pi^+\pi^-\pi^+\pi^-$ events. However, none of these background sources peak close to the η' signal in the $\pi^+\pi^-\pi^+\pi^-$ mass spectrum.

For $J/\psi \rightarrow \gamma\eta'$ with $\eta' \rightarrow \pi^+\pi^-\pi^0\pi^0$ (Mode II), candidate events must have two charged tracks with zero net charge and at least five photons. The charged tracks also need to successfully pass the IP vertex fit. To reconstruct the π^0 candidate, a one-constraint (1C) kinematic fit is performed on each photon pair with the invariant mass

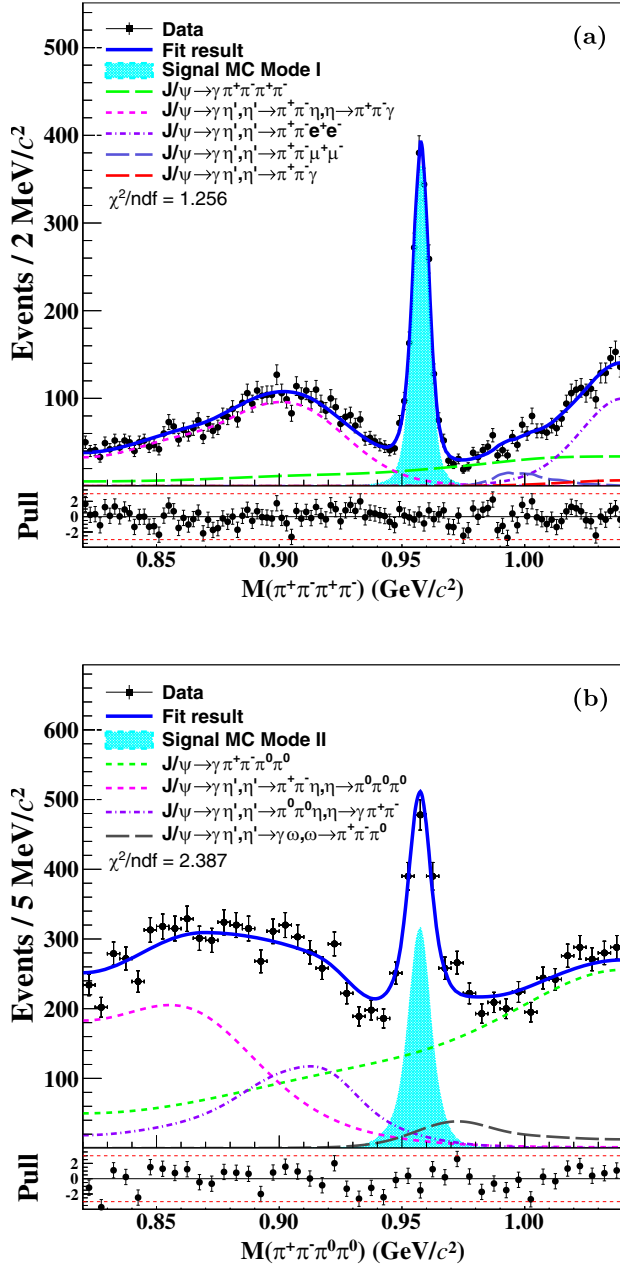


FIG. 1. The fit results of the mass spectra of $\pi^+\pi^-\pi^+\pi^-$ (a) and $\pi^+\pi^-\pi^0\pi^0$ (b).

constrained to the known π^0 mass, and $\chi^2_{1C}(\gamma\gamma) < 50$ is required. Then a six-constraint (6C) kinematic fit to the initial e^+e^- four momentum and the nominal π^0 masses for two $\gamma\gamma$ pairs is performed under the hypothesis of $J/\psi \rightarrow \gamma\pi^+\pi^-\pi^0\pi^0$ in which the two π^0 masses are constrained. For events with more than two π^0 candidates, the combination with the smallest χ^2_{6C} is retained, and $\chi^2_{6C} < 35$ is required to exclude events kinematically incompatible with the signal hypothesis. To reject backgrounds with six photons in the final state, a 6C kinematic fit under the hypothesis of $J/\psi \rightarrow \gamma\gamma\pi^+\pi^-\pi^0\pi^0$ is also made and the χ^2_{6C} is required to

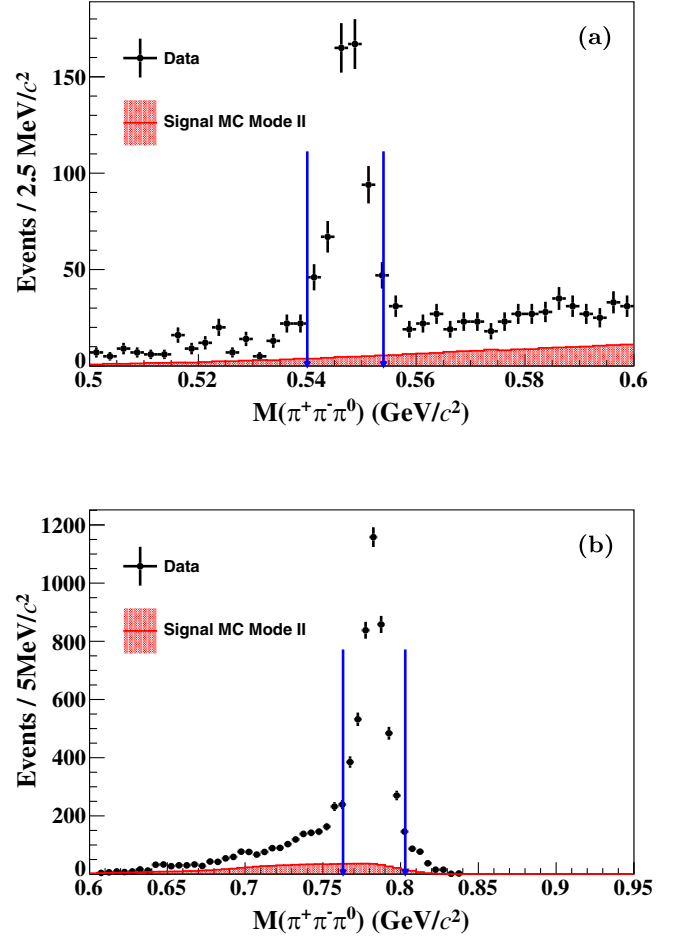


FIG. 2. The distributions of the $\pi^+\pi^-\pi^0$ invariant masses closest to the known masses of (a) η and (b) ω . The blue arrows mark the interval for rejecting each resonance. The signal MC is displayed with arbitrary normalization.

be greater than that of the signal hypothesis $\gamma\pi^+\pi^-\pi^0\pi^0$. Figures 2(a) and 2(b) show the invariant-mass spectra of the $\pi^+\pi^-\pi^0$ combination passing this selection and lying closest to the known η (ω) mass (denoted as m_η/m_ω), respectively, where the η and ω peaks are evident. To reject background events with η (ω) in the final states, the combination closest to m_η (m_ω) is required to satisfy $|M(\pi^+\pi^-\pi^0) - m_\eta| > 0.007 \text{ GeV}/c^2$ ($|M(\pi^+\pi^-\pi^0) - m_\omega| > 0.02 \text{ GeV}/c^2$).

Figure 1(b) shows the $\pi^+\pi^-\pi^0\pi^0$ invariant mass for events satisfying the above requirements, in which a clean η' peak is evident. The same selection is performed on the inclusive MC sample of 10 billion J/ψ events to investigate possible sources of contamination. The dominant backgrounds are found to arise from $\eta' \rightarrow \pi^+\pi^-\eta$, $\eta \rightarrow \pi^0\pi^0\pi^0$, $\eta' \rightarrow \pi^0\pi^0\eta$, $\eta \rightarrow \gamma\pi^+\pi^-$, $\eta' \rightarrow \gamma\omega$, $\omega \rightarrow \pi^+\pi^-\pi^0$ and non-resonant $J/\psi \rightarrow \gamma\pi^+\pi^-\pi^0\pi^0$ events. None of these background channels peak in the η' signal region.

When selecting $J/\psi \rightarrow \gamma\eta'$ with $\eta' \rightarrow 4\pi^0$ (Mode III) events, a one-constraint (1C) kinematic fit is performed on

TABLE I. The fitted signal yields (or 90% confidence level upper limit), the detection efficiencies and the measured branching fractions (or 90% confidence level upper limit). Also shown are the previous BESIII results.

Mode	N	$\epsilon(\%)$	$\mathcal{B}(\eta' \rightarrow X)$	Previous BESIII result [3,9]
$\eta' \rightarrow \pi^+\pi^-\pi^+\pi^-$	1650 ± 48	36.4	$(8.56 \pm 0.25(\text{stat}) \pm 0.23(\text{syst})) \times 10^{-5}$	$(8.53 \pm 0.69(\text{stat}) \pm 0.64(\text{syst})) \times 10^{-5}$
$\eta' \rightarrow \pi^+\pi^-\pi^0\pi^0$	865 ± 49	7.8	$(2.12 \pm 0.12(\text{stat}) \pm 0.10(\text{syst})) \times 10^{-4}$	$(1.82 \pm 0.35(\text{stat}) \pm 0.18(\text{syst})) \times 10^{-4}$
$\eta' \rightarrow \pi^0\pi^0\pi^0\pi^0$	<10	1.6	$<1.24 \times 10^{-5}$	$<4.94 \times 10^{-5}$

the π^0 candidates reconstructed from photon pairs with the invariant mass of the two photons constrained to the π^0 mass, with the requirement $\chi_{1C}^2(\gamma\gamma) < 10$. A further eight-constraint (8C) kinematic fit to the initial e^+e^- four momentum and the nominal π^0 masses for four $\gamma\gamma$ pairs is performed to the $\gamma\pi^0\pi^0\pi^0\pi^0$ hypothesis by enforcing energy-momentum conservation and constraining the invariant mass of each of the four photon pairs to the known π^0 mass. If more than one candidate combination is found, that one with the smallest χ_{8C}^2 is retained. Candidate events with $\chi_{8C}^2 > 40$ are rejected to exclude events that are kinematically incompatible with the signal hypothesis. An additional requirement of $|M(\pi^0\pi^0\pi^0) - m_\eta| > 0.02 \text{ GeV}/c^2$ is used to remove the η background events, where $M(\pi^0\pi^0\pi^0)$ is the combination of the $\pi^0\pi^0\pi^0$ invariant mass closest to the known mass of the η meson.

To reject background with 10 or 11 photons in the final states, the χ_{4C}^2 of the 4C kinematic fit to signal hypothesis is required to be less than those of the 4C kinematic fits to both the 10 and 11 photon hypotheses. To investigate possible sources of contamination, we apply these selections to the inclusive MC sample of 10 billion J/ψ events and find that the only significant backgrounds come from $\eta' \rightarrow \pi^0\pi^0\eta$, $\eta \rightarrow \pi^0\pi^0\pi^0$ and nonresonant $J/\psi \rightarrow \gamma\pi^0\pi^0\pi^0\pi^0$ events.

IV. MEASUREMENT OF $\mathcal{B}(\eta' \rightarrow \pi^+\pi^-\pi^+\pi^-)$

The signal yields of the exclusive channels are obtained by performing unbinned maximum likelihood fits to the mass spectra of the selected $\eta' \rightarrow \pi^+\pi^-\pi^+\pi^-$ and $\eta' \rightarrow \pi^+\pi^-\pi^0\pi^0$ candidates, respectively. In the fits, the signal components are modeled by the MC-simulated shape convolved with a Gaussian function to account for the difference in the mass resolution between data and MC simulation. The background components considered are subdivided into two classes: (i) the shapes of those background events that contribute to a structure in $M(\pi^+\pi^-\pi^+\pi^-)$ (e.g. $\eta' \rightarrow \pi^+\pi^-\eta$ with $\eta \rightarrow \gamma\pi^+\pi^-$ and $\eta' \rightarrow \pi^+\pi^-e^+e^-$) or $M(\pi^+\pi^-\pi^0\pi^0)$ (e.g. $\eta' \rightarrow \pi^+\pi^-\eta$ with $\eta \rightarrow \pi^0\pi^0\pi^0$ and $\eta' \rightarrow \pi^0\pi^0\eta$ with $\eta \rightarrow \gamma\pi^+\pi^-$, as well as $\eta' \rightarrow \gamma\omega$ with $\omega \rightarrow \pi^+\pi^-\pi^0$) are taken from the dedicated MC simulations; and (ii) $J/\psi \rightarrow \gamma\pi^+\pi^-\pi^+\pi^-$ and $J/\psi \rightarrow \gamma\pi^+\pi^-\pi^0\pi^0$ nonresonant decays are described with the MC-simulated shape in uniform phase-space model. The magnitudes of the different components are left free in the fit to

account for the uncertainties of the branching fractions of $J/\psi \rightarrow \gamma\eta'$ and other intermediate decays (e.g. $\eta' \rightarrow \pi^+\pi^-\eta$, $\eta' \rightarrow \pi^0\pi^0\eta$, and $\eta \rightarrow \gamma\pi^+\pi^-$). The fits, as shown in Fig. 1, yield 1650 ± 48 events for $\eta' \rightarrow \pi^+\pi^-\pi^+\pi^-$ and 865 ± 49 events for $\eta' \rightarrow \pi^+\pi^-\pi^0\pi^0$, where the goodness-of-fit is 1.256 and 2.387, respectively.

The branching fraction of each channel is calculated as

$$\mathcal{B}(X) = \frac{N_{\text{signal}}(X)}{N_{J/\psi} \cdot \prod \mathcal{B}_i \cdot \epsilon(X)}, \quad (1)$$

where X represents Mode I or Mode II. $N_{\text{signal}}(X)$ is the number of signal events. $N_{J/\psi}$ is the number of J/ψ events. $\prod \mathcal{B}_i$ is the product branching fractions of all the intermediate states quoted from the PDG [17] in each channel, which is $\mathcal{B}(J/\psi \rightarrow \gamma\eta')$ for Mode I and $\mathcal{B}(J/\psi \rightarrow \gamma\eta') \cdot \mathcal{B}^2(\pi^0 \rightarrow \gamma\gamma)$ for Mode II. $\epsilon(X)$ is the detection efficiency obtained from the MC simulation with the ChPT and VMD model [4]. The measured branching fractions of these two decay modes, as summarized in Table I, are consistent with previous results [3] obtained from a dataset of 1.3 billion J/ψ events, which is a subset of the sample used in the current analysis.

V. AMPLITUDE ANALYSIS OF $\eta' \rightarrow \pi^+\pi^-\pi^+\pi^-$

To investigate the doubly virtual isovector contribution, an amplitude analysis of $\eta' \rightarrow \pi^+\pi^-\pi^+\pi^-$ is necessary. Given the limited sample size and high background level for $\eta' \rightarrow \pi^+\pi^-\pi^0\pi^0$ decays, we only perform an amplitude analysis of $\eta' \rightarrow \pi^+(p_1)\pi^-(p_2)\pi^+(p_3)\pi^-(p_4)$. The decay amplitude is constructed with a combination of the ChPT and VMD model [4], as described by

$$\begin{aligned} \mathcal{A}(\eta' \rightarrow \pi^+\pi^-\pi^+\pi^-) &= \epsilon_{\mu\nu\alpha\beta} p_1^\mu p_2^\nu p_3^\alpha p_4^\beta \\ &\times \left\{ \left[\frac{s_{12}}{D_\rho(s_{12})} + \frac{s_{34}}{D_\rho(s_{34})} - \frac{s_{14}}{D_\rho(s_{14})} - \frac{s_{23}}{D_\rho(s_{23})} \right] \right. \\ &\left. + \alpha \left[\frac{M_\rho^2(s_{12} + s_{34})}{D_\rho(s_{12})D_\rho(s_{34})} - \frac{M_\rho^2(s_{14} + s_{23})}{D_\rho(s_{14})D_\rho(s_{23})} \right] \right\}, \quad (2) \end{aligned}$$

where

$$D_\rho(s) = M_\rho^2 - s - iM_\rho\Gamma_\rho(s), \quad (3)$$

$$\Gamma_\rho(s) = \frac{M_\rho}{\sqrt{s}} \left(\frac{s - 4M_\pi^2}{M_\rho^2 - 4M_\pi^2} \right)^{3/2} \Gamma_\rho, \quad (4)$$

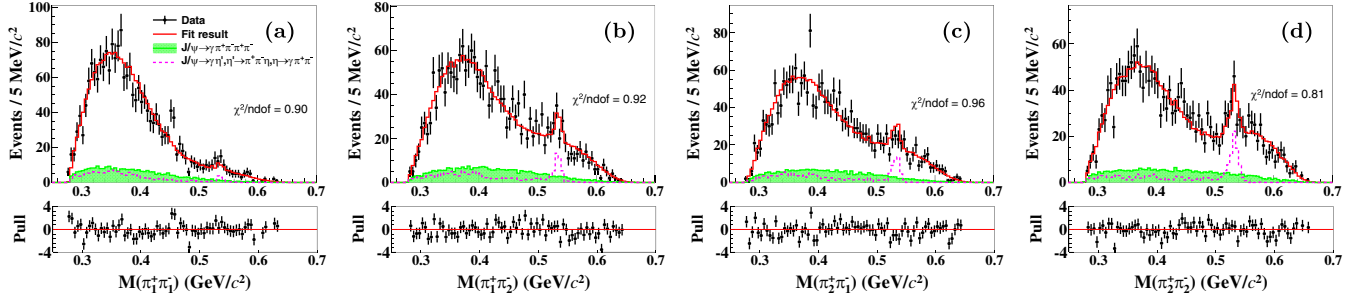


FIG. 3. The fitted projections to the invariant mass of four $\pi^+\pi^-$ combinations, where $\pi_1^{+(-)}$ and $\pi_2^{+(-)}$ are sorted in ascending order of their energy.

is the inverse ρ propagator (M_ρ and Γ_ρ are the mass and width of ρ meson), and $s_{12} = (p_1 + p_2)^2$ and $s_{34} = (p_3 + p_4)^2$ are the invariant-masses squared of two independent $\pi^+\pi^-$ pairs; α corresponds to $\frac{c_3}{c_1 - c_2}$ in Ref. [4] since the fit is only sensitive to this ratio rather than the individual parameters, where c_i represent the relative contributions of distinct decay mechanisms.

The free parameters of the probability-density function (PDF) to observe the i th event characterized by the measured four-momenta ξ_i of the particles in the final state is

$$\mathcal{P}(\xi_i) = \frac{|\mathcal{A}(\xi_i)|^2 \epsilon(\xi_i)}{\int |\mathcal{A}(\xi)|^2 \epsilon(\xi) d\xi}, \quad (5)$$

where \mathcal{A} is the amplitude as shown in Eq. (2), and $\epsilon(\xi_i)$ is the detection efficiency. The parameters are optimized with an unbinned maximum likelihood fit using the sample of selected $\eta' \rightarrow \pi^+\pi^-\pi^+\pi^-$ events, a total of 2047 events found in the η' mass region of $0.94 \text{ GeV}/c^2 < M(\pi^+\pi^-\pi^+\pi^-) < 0.97 \text{ GeV}/c^2$. The fit minimizes the negative log-likelihood value

$$-\ln \mathcal{L} = -\omega' \left[\sum_{i=1}^{N_{\text{data}}} \ln \mathcal{P}(\xi_i) - \omega_{\text{bkg1}} \sum_{j=1}^{N_{\text{bkg1}}} \ln \mathcal{P}(\xi_j) - \omega_{\text{bkg2}} \sum_{k=1}^{N_{\text{bkg2}}} \ln \mathcal{P}(\xi_k) \right], \quad (6)$$

where \mathcal{P} is the PDF, i, j and k run over all accepted data, the continuous background $J/\psi \rightarrow \gamma\pi^+\pi^-\pi^+\pi^-$ and the peaking background $J/\psi \rightarrow \gamma\eta', \eta' \rightarrow \pi^+\pi^-\eta, \eta \rightarrow \gamma\pi^+\pi^-$ events, respectively, and their corresponding number of events are denoted by N_{data} , N_{bkg1} and N_{bkg2} , with the backgrounds modeled by MC simulation. Here, $\omega_{\text{bkg1}} = \frac{N'_{\text{bkg1}}}{N_{\text{bkg1}}}$ and $\omega_{\text{bkg2}} = \frac{N'_{\text{bkg2}}}{N_{\text{bkg2}}}$ are the weights of the backgrounds, where N'_{bkg1} and N'_{bkg2} are their contributions in the signal region according to the above fit results as displayed in Fig. 1(a). To obtain an unbiased uncertainty

estimation, the normalization factor derived from Ref. [22] is considered, described as

$$\omega' = \frac{N_{\text{data}} - N_{\text{bkg1}}\omega_{\text{bkg1}} - N_{\text{bkg2}}\omega_{\text{bkg2}}}{N_{\text{data}} + N_{\text{bkg1}}\omega_{\text{bkg1}}^2 + N_{\text{bkg2}}\omega_{\text{bkg2}}^2}. \quad (7)$$

To simplify the fit, the mass and width of the ρ are fixed at the world-average values [17], $M_\rho = 775.11 \text{ MeV}/c^2$ and $\Gamma_\rho = 149.1 \text{ MeV}/c^2$. The amplitude analysis fit gives $\alpha = 1.22 \pm 0.33$, where the uncertainty is statistical only. Projections of the data and fit results to the mass spectra of different $\pi^+\pi^-$ combinations are displayed in Fig. 3, which indicates that the amplitude fit provides a good description of the data. An alternative fit with free resonant parameters of ρ is also performed, which returns a fitted mass $M_\rho = 671.9 \pm 13.4 \text{ MeV}/c^2$ and width $\Gamma_\rho = 233.7 \pm 16.7 \text{ MeV}/c^2$ that deviate significantly from the world-average values. In this case, we also find that the fit result for α is not stable. The notable deviations of resonant parameters and unstable value of alpha stem from the similar lineshape of the terms with and without α in Eq. (2), which leads to a strong correlation between them. Thus, the fit with the fixed ρ parameters is taken as the baseline. This measurement is in good agreement with the prediction of unity from the combined ChPT and VMD model in Ref. [4], where $c_3 = 1$ and $c_1 - c_2 = 1$.

VI. SEARCH FOR $\eta' \rightarrow 4\pi^0$

No significant signal contribution is evident for the decay $\eta' \rightarrow 4\pi^0$ in the $M(4\pi^0)$ distribution shown in Fig. 4(a). To quantify this conclusion, an unbinned maximum-likelihood fit is performed on the $4\pi^0$ mass spectrum, allowing for background contributions and a possible signal component. The total PDF consists of a signal component, the peaking and nonpeaking background contributions. The signal component is modeled as the MC simulated shape. Both the peaking and nonpeaking background contributions from $J/\psi \rightarrow \gamma\eta', \eta' \rightarrow \pi^0\pi^0\eta, \eta \rightarrow \pi^0\pi^0\pi^0$ and $J/\psi \rightarrow \gamma\pi^0\pi^0\pi^0\pi^0$ are also described with shapes obtained from the dedicated MC simulation.

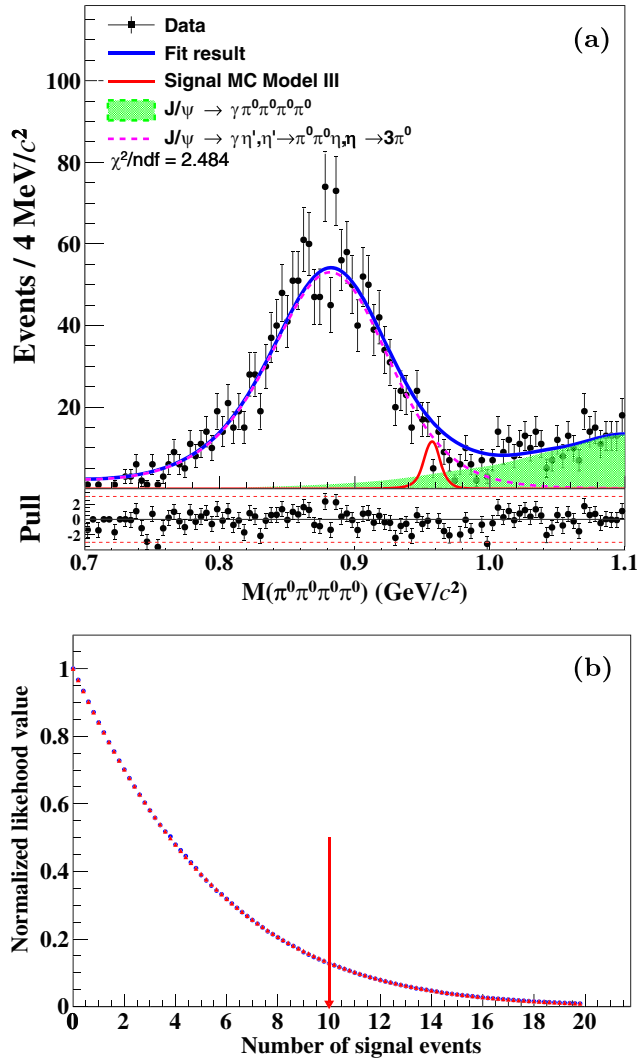


FIG. 4. The fit result to the $4\pi^0$ invariant mass (a) and the normalized likelihood distribution (b). In (b), the blue dots and red triangles are the likelihood distributions before and after convolution with a Gaussian function with resolution equal to the total systematic uncertainty, respectively. The red arrow indicates the upper limit at the 90% confidence level.

A Bayesian approach [23] is used to determine an upper limit on the branching fraction of $\eta' \rightarrow 4\pi^0$. A series of fits are performed for different assumed values N of the signal yield shown in Fig. 4(b), and the negative log-likelihood \mathcal{S} is determined for each fit.

The distribution of normalized likelihood values, defined as $\mathcal{L}(N) = \exp(-[\mathcal{S}(N) - \mathcal{S}_{\min}])$, where \mathcal{S}_{\min} is the normalized minimum negative log-likelihood obtained from the ensemble of fits at $N = 0$, is taken as the PDF for the likelihood function $\mathcal{L}(N)$. The upper limit on the number of signal events, N_{UL} , is determined at 90% of the integral of the PDF

$$\frac{\int_0^{N_{\text{UL}}} \mathcal{L}(N) dN}{\int_0^{\infty} \mathcal{L}(N) dN} = 0.9, \quad (8)$$

where N is the fitted number of signal events. To account for the additive systematic uncertainties related to the fits, several alternative fits are performed. These alternative fits involve different fit ranges, continuum background shapes and peaking background shapes. Among the results of these fits, the largest number of signal events 9.9 is chosen. With this upper limit of $N_{\text{UL}} = 9.9$, the upper limit on the branching fraction is calculated with

$$\mathcal{B}(\eta' \rightarrow 4\pi^0) < \frac{N_{\text{UL}}}{N_{J/\psi} \cdot \mathcal{B}(J/\psi \rightarrow \gamma\eta') \cdot \mathcal{B}^4(\pi^0 \rightarrow \gamma\gamma) \cdot \epsilon}, \quad (9)$$

where ϵ is the detection efficiency obtained by MC simulation. Then the upper limit for the branching fraction at the 90% confidence level is determined to be $\mathcal{B}_{\text{UL}} = 1.22 \times 10^{-5}$.

VII. SYSTEMATIC UNCERTAINTY

Sources of systematic uncertainties and their corresponding contributions to the measurements of the branching fractions for the different decay modes are summarized in Table II. The total systematic uncertainties are obtained by adding all the contributions in quadrature under the assumption that they are independent.

The MDC tracking efficiency is studied using a clean control sample of $J/\psi \rightarrow \pi^+\pi^-\pi^0$ decays. It is found that the MC simulation agrees with data within 0.5% for each charged track. The systematic uncertainties on the tracking efficiency are taken as 2% and 1%, for Mode I and Mode II, respectively.

The photon-detection efficiency is studied with a dedicated sample of the $e^+e^- \rightarrow \gamma\mu^+\mu^-$ events. The difference in efficiencies between data and MC simulation, 0.5%, is taken as the corresponding systematic uncertainty.

Uncertainties associated with the kinematic fits for the charged decay Mode I and Mode II come from the inconsistency of the track helix parameters between data

TABLE II. The systematic uncertainties on the branching-fraction measurements (in %).

Source	Mode I	Mode II	Mode III
MDC tracking	2	1	...
Photon detection	0.5	2.5	4.5
Kinematic fit	0.6	0.2	5.6
Peaking background	0.4	0.1	...
Continuous background	0.2	1.6	...
Veto $\eta(\omega)$ signal	...	2.8	...
Veto $\eta \rightarrow 3\pi^0$	3.0
$\mathcal{B}(J/\psi \rightarrow \gamma\eta')$	1.3	1.3	1.3
$\mathcal{B}(\pi^0 \rightarrow \gamma\gamma)$...	0.06	0.12
$N_{J/\psi}$	0.44	0.44	0.44
Generator model	0.8	0.6	0.1
Total	2.7	4.5	8.0

and MC simulation. The helix parameters for the charged tracks of the MC samples are corrected to eliminate this inconsistency, as described in Ref. [24], and the agreement of χ^2 distributions between data and MC simulation is much improved. We take half of the differences on the selection efficiencies with and without the correction as the systematic uncertainties, which are 0.6% and 0.2% for Mode I and Mode II, respectively. The uncertainty for Mode III associated with the kinematic fit is estimated by adjusting the components of the photon-energy error matrix in the signal MC sample to reflect the known difference in resolution between data and MC simulation [25] and the difference is estimated to be 5.6%.

Uncertainties arise from the understanding of the background associated with the estimation of the resonant and nonresonant background events. For the background contributions from the phase-space events, e.g., $J/\psi \rightarrow \gamma\pi^+\pi^-\pi^+\pi^-$ and $J/\psi \rightarrow \gamma\pi^+\pi^-\pi^0\pi^0$, alternative fits are performed by replacing phase-space MC shapes with a third-order Chebychev function. The deviations in signal yields after implementing these modifications are found to be 0.2% and 1.6% for Mode I and Mode II, respectively. The uncertainties due to peaking background events below or just above the η' peak are considered by fixing these contributions according to the branching fractions of $J/\psi \rightarrow \gamma\eta'$ and the cascade decays, and lead to uncertainties of 0.4% and 0.1%, respectively.

The uncertainty associated with the η and ω veto is studied by varying the η and ω mass requirements, and is assigned to be 2.8% for mode II. The uncertainty from the MC model is estimated by varying the parameters in the ChPT and VMD model, and the largest difference in the detection efficiencies is assigned as the systematic uncertainty, which is 0.8% for mode I, 0.6% for Mode II and 0.1% for Mode III. Similarly, the systematic uncertainty associated with vetoing η signal in Mode III is estimated to be 3.0%. The uncertainties in the branching fractions of $J/\psi \rightarrow \gamma\eta'$ and $\pi^0 \rightarrow \gamma\gamma$ are 1.3% and 0.06%, respectively. The uncertainty due to the total number of J/ψ events ($N_{J/\psi}$) is 0.44% [10].

The systematic uncertainties on the doubly virtual isovector contribution α from the amplitude analysis of $\eta' \rightarrow \pi^+\pi^-\pi^+\pi^-$ are summarized in Table III. The uncertainty in the pion tracking efficiency is studied using a control sample of $J/\psi \rightarrow \pi^+\pi^-\pi^0$ decays. The data-MC difference is extracted as a function of the particle momentum and the cosine of the polar angle, and then a reweighting procedure is applied on the charged pions for each event to calculate the MC integral cross section. Following this, an alternative amplitude analysis is conducted and the difference between the results with and without correction, 0.1%, is assigned as the systematic uncertainty. For the continuum background from $J/\psi \rightarrow \gamma\pi^+\pi^-\pi^+\pi^-$, by replacing with a third-order Chebychev polynomial function in the fit, the normalized background

TABLE III. The systematic uncertainties on the doubly virtual isovector contribution α to $\eta' \rightarrow \pi^+\pi^-\pi^+\pi^-$ (in %).

Source	$\eta' \rightarrow \pi^+\pi^-\pi^+\pi^-$
MDC tracking	0.1
4C kinematic fit	0.5
Continuum background	2.0
Peaking background	2.9
Mass of ρ	0.7
Width of ρ	0.2
Total	3.6

events is found to be 273 ± 17 . An alternative amplitude fit is performed and the change in α with respect to the nominal result, 2.0%, is taken as the systematic uncertainty. The uncertainty from peaking background associated with the background events ($J/\psi \rightarrow \gamma\eta'$, $\eta' \rightarrow \pi^+\pi^-\eta$, $\eta \rightarrow \gamma\pi^+\pi^-$) is estimated by normalizing the number of background events to be 178 ± 13 in the amplitude analysis in accordance with the branching fractions of $J/\psi \rightarrow \gamma\eta'$ and the cascade decays [17]. The change of result, 2.9%, is taken as the systematic uncertainty. The systematic uncertainties associated with the mass and width of ρ , are estimated by varying the range by $\pm 1\sigma$ instead of fixing to the world average values, which are determined to be 0.7% and 0.2%, respectively. The total systematic uncertainty of 3.6% is obtained by adding all systematic uncertainties in quadrature assuming that they are independent.

VIII. BRANCHING-FRACTION RESULTS

After taking into account the systematic uncertainties, the branching fractions of $\eta' \rightarrow \pi^+\pi^-\pi^+\pi^-$ and $\eta' \rightarrow \pi^+\pi^-\pi^0\pi^0$ are measured to be $(8.56 \pm 0.25(\text{stat}) \pm 0.23(\text{syst})) \times 10^{-5}$ and $(2.12 \pm 0.12(\text{stat}) \pm 0.10(\text{syst})) \times 10^{-4}$, respectively, where the first uncertainties are statistical and the second systematic. No $\eta' \rightarrow 4\pi^0$ signal is observed and the upper limit on its decay branching fraction, considering only additive systematic uncertainties is found to be $\mathcal{B}_{\text{UL}} = 1.22 \times 10^{-5}$ at the 90% confidence level. The final upper limit on the branching fraction also considers the multiplicative systematic uncertainty, which is accounted for by convolving the likelihood distribution $L(N)$ to obtain the smeared likelihood $L'(N)$,

$$L'(N) = \int_0^1 L\left(\frac{S}{\hat{S}}N\right) \exp\left[-\frac{(S - \hat{S})}{2\sigma_S^2}\right] dS. \quad (10)$$

In this expression \hat{S} is the nominal efficiency, σ_S is its systematical uncertainty (8%) coming from Table II and N is the number of signal events for $\eta' \rightarrow 4\pi^0$. Following this procedure, the upper limit on the number of signal events at the 90% confidence level is set to be 10 as shown in Fig. 4(b),

and the corresponding upper limit of the branching fraction is $\mathcal{B}(\eta' \rightarrow 4\pi^0) < 1.24 \times 10^{-5}$.

IX. SUMMARY

In summary, using a sample of $(10087 \pm 44) \times 10^6 J/\psi$ events, we perform improved measurements of the branching fractions of $\eta' \rightarrow \pi^+\pi^-\pi^+\pi^-$ and $\eta' \rightarrow \pi^+\pi^-\pi^0\pi^0$ decays with $J/\psi \rightarrow \gamma\eta'$. The measured branching fractions of these two decays are in good agreement with the previous works [3], with a three-times improvement in precision. In addition, within the framework of the ChPT and VMD model, an amplitude analysis of $\eta' \rightarrow \pi^+\pi^-\pi^+\pi^-$ is performed for the first time to investigate the doubly virtual isovector contribution. The parameter α , corresponding to $\frac{c_1-c_2}{c_3}$ in Ref. [4], is determined to be $1.22 \pm 0.33(\text{stat}) \pm 0.04(\text{syst})$, which is consistent with the prediction of theoretical calculations [4].

We have also searched for the rare decay $\eta' \rightarrow 4\pi^0$, and no evidence is found. The upper limit of $\mathcal{B}(\eta' \rightarrow 4\pi^0)$ at the 90% confidence level is determined to be 1.24×10^{-5} , thereby improving on the previous limit [9] by a factor of four.

ACKNOWLEDGMENTS

The BESIII Collaboration thanks the staff of BEPCII and the IHEP computing center for their strong support. This work is supported in part by National Key R&D Program of China under Contracts No. 2020YFA0406300 and No. 2020YFA0406400; National Natural Science Foundation of China (NSFC) under Contracts No. 11635010, No. 11735014, No. 11835012, No. 11935015, No. 11935016, No. 11935018,

No. 11961141012, No. 12025502, No. 12035009, No. 12035013, No. 12061131003, No. 12075250, No. 12192260, No. 12192261, No. 12192262, No. 12192263, No. 12192264, No. 12192265, No. 12221005, No. 12225509, and No. 12235017; the Chinese Academy of Sciences (CAS) Large-Scale Scientific Facility Program; the CAS Center for Excellence in Particle Physics (CCEPP); Joint Large-Scale Scientific Facility Funds of the NSFC and CAS under Contract No. U1832207; CAS Key Research Program of Frontier Sciences under Contracts No. QYZDJ-SSW-SLH003 and No. QYZDJ-SSW-SLH040; 100 Talents Program of CAS; The Institute of Nuclear and Particle Physics (INPAC) and Shanghai Key Laboratory for Particle Physics and Cosmology; European Union's Horizon 2020 research and innovation programme under Marie Skłodowska-Curie grant agreement under Contract No. 894790; German Research Foundation DFG under Contracts No. 455635585, Collaborative Research Center CRC 1044, No. FOR5327, and No. GRK 2149; Istituto Nazionale di Fisica Nucleare, Italy; Ministry of Development of Turkey under Contract No. DPT2006K-120470; National Research Foundation of Korea under Contract No. NRF-2022R1A2C1092335; National Science and Technology fund of Mongolia; National Science Research and Innovation Fund (NSRF) via the Program Management Unit for Human Resources & Institutional Development, Research and Innovation of Thailand under Contract No. B16F640076; Polish National Science Centre under Contract No. 2019/35/O/ST2/02907; The Swedish Research Council; U.S. Department of Energy under Contract No. DE-FG02-05ER41374.

-
- [1] T. Aoyama *et al.*, *Phys. Rep.* **887**, 1 (2020).
 [2] S. S. Fang, *Natl. Sci. Rev.* **8**, 11 (2021).
 [3] M. Ablikim *et al.* (BESIII Collaboration), *Phys. Rev. Lett.* **112**, 251801 (2014).
 [4] F. K. Guo, Bastian Kubis, and Andreas Wirzba, *Phys. Rev. D* **85**, 014014 (2012).
 [5] A. Pich and E. Rafael, *Nucl. Phys.* **B367**, 313 (1991).
 [6] K. Otnad, B. Kubis, U. G. Meißner, and F. K. Guo, *Phys. Lett. B* **687**, 42 (2010).
 [7] S. V. Donskov, V. N. Kolosov, A. A. Lednev, Y. V. Mikhailov, V. A. Polyakov, V. D. Samoylenko, and G. V. Khaustov (GAMS Collaboration), *Mod. Phys. Lett. A* **29**, 1450213 (2014).
 [8] D. Alde *et al.*, *Z. Phys. C* **36**, 603 (1987).
 [9] M. Ablikim *et al.* (BESIII Collaboration), *Phys. Rev. D* **101**, 032001 (2020).
 [10] M. Abikim *et al.* (BESIII Collaboration), *Chin. Phys. C* **46**, 074001 (2022).
 [11] M. Ablikim *et al.* (BESIII Collaboration), *Nucl. Instrum. Methods Phys. Res., Sect. A* **614**, 345 (2010).
 [12] C. Yu, Z. Duan, S. Gu, Y. Guo, X. Huang, D. Ji, H. Ji, Y. Jiao, Z. Liu, Y. Peng *et al.*, in *Proceedings of IPAC2016, Busan, Korea* (JACoW, Busan, 2016), <https://accelconf.web.cern.ch/ipac2016/doi/JACoW-IPAC2016-TUYA01.html>.
 [13] M. Ablikim *et al.* (BESIII Collaboration), *Chin. Phys. C* **44**, 040001 (2020).
 [14] S. Agostinelli *et al.* (GEANT4 Collaboration), *Nucl. Instrum. Methods Phys. Res., Sect. A* **506**, 250 (2003).
 [15] S. Jadach, B. F. L. Ward, and Z. Was, *Comput. Phys. Commun.* **130**, 260 (2000); *Phys. Rev. D* **63**, 113009 (2001).
 [16] D. J. Lange, *Nucl. Instrum. Methods Phys. Res., Sect. A* **462**, 152 (2001); R. G. Ping, *Chin. Phys. C* **32**, 599 (2008).

- [17] R. L. Workman *et al.* (Particle Data Group), *Prog. Theor. Exp. Phys.* **2022**, 083C01 (2022).
- [18] J. C. Chen, G. S. Huang, X. R. Qi, D. H. Zhang, and Y. S. Zhu, *Phys. Rev. D* **62**, 034003 (2000).
- [19] E. Richter-Was, *Phys. Lett. B* **303**, 163 (1993).
- [20] Y. H. Guan, X. R. Lu, Y. H. Zheng, and Y. F. Wang, *Chin. Phys. C* **38**, 016201 (2014); E. Richter-Was, *Phys. Lett. B* **303**, 163 (1993).
- [21] X. Y. Zhou, S. X. Du, G. Li, and C. P. Shen, *Comput. Phys. Commun.* **258**, 107540 (2021).
- [22] C. Langenbruch, *Eur. Phys. J. C* **82**, 393 (2022).
- [23] Y. S. Zhu, *Chin. Phys. C* **32**, 363 (2008).
- [24] M. Ablikim *et al.* (BESIII Collaboration), *Phys. Rev. D* **87**, 012002 (2013).
- [25] M. Ablikim *et al.* (BESIII Collaboration), *Phys. Rev. D* **94**, 072005 (2016).